IOP Publishing Plasma Sources Science and Technology

Plasma Sources Sci. Technol. **23** (2014) 015001 (8pp) doi:10.1088/0963-0252/23/1/015001

Ion distribution functions at the electrodes of capacitively coupled high-pressure hydrogen discharges

Edmund Schüngel[1], Sebastian Mohr[1], Julian Schulze[1], Uwe Czarnetzki[1] and Mark J Kushner[2]

[1] Insitute for Plasma and Atomic Physics, Ruhr-University Bochum, 44780 Bochum, Germany
[2] Department of Electrical Engineering and Computer Science, University of Michigan, Ann Arbor, MI 48109-2122, USA

E-mail: Edmund.Schuengel@ep5.rub.de

Received 24 June 2013, revised 24 October 2013
Accepted for publication 5 November 2013
Published 16 December 2013

Abstract

The flux-energy distribution functions of H_3^+ ions at the electrodes of capacitively coupled parallel plate discharges operated in a regime of relatively high gas pressures (200–650 Pa) are investigated experimentally using (differentially pumped) energy-resolved mass spectrometry under various conditions and compared with the results of a numeric simulation and a model. It is shown that the simulated distribution function can be reproduced by a simple analytical modeling approach, which assumes a constant collision frequency and is valid for highly collisional sheaths. The comparison between experiment and simulation reveals that not the entire angular distribution is covered by the diagnostics. However, the normalized experimentally obtained distributions are close to the simulated ones, thus indicating that the measurements allow for a reasonable discussion. In a single frequency 13.56 MHz discharge, the width of the distribution increases as a function of the voltage amplitude and decreases as a function of pressure. Applying an electrically asymmetric voltage waveform (13.56 MHz + 27.12 MHz) to the powered electrode breaks the symmetry of the geometrically symmetric discharge. This allows manipulation of the shape and width of the ion flux-energy distribution functions at the electrodes by tuning the phase angle between the two frequencies. It is found experimentally that controlling the ion energy without affecting the total flux is possible via the electrical asymmetry effect under these high-pressure conditions, whereas a change in pressure or voltage amplitude affects both the energy and the flux of ions.

(Some figures may appear in colour only in the online journal)

1. Introduction

The ion flux-energy distribution function (IDF) at the surfaces is of substantial importance for processing applications of capacitively coupled radio frequency (CCRF) discharges [1, 2]. For instance, the selective and anisotropic etching of micro-electronic devices requires a high and directed ion velocity. Therefore, asymmetric chamber configurations with a large voltage drop across the sheath adjacent to the wafer and low pressure conditions are typically used [3–5]. For the deposition of thin films a high flux of ions with low energy is usually desired [6–12]. Accordingly, a relatively high-pressure process is performed in a symmetric discharge. The idea is to reduce the film stress caused by the highly energetic ion bombardement [13, 14] without lowering the plasma density and, hence, the deposition rate or losing the contribution of the charged species to the deposition process.

More advanced strategies include the control of the IDF via additional substrate biasing [15], pulsing [16] or driving voltage waveforms consisting of multiple frequencies. In the latter case the driving voltage may consist of two substantially different frequencies, allowing one to control the ion energy with the voltage amplitude of the low-frequency component and the total ion flux with the voltage amplitude

of the high-frequency component [5, 17, 18]. This separate control is, however, strongly limited by the frequency coupling [19–21] and the effect of secondary electrons [22–24]. Recently, an alternative approach has been proposed: using two consecutive harmonics generating an asymmetric voltage waveform [25], that is given by

$$\phi(t) = \phi_0 \tfrac{1}{2} \left[\cos(\omega_{\mathrm{rf}} t + \theta) + \cos(2\omega_{\mathrm{rf}} t)\right]. \qquad (1)$$

ϕ_0 and θ are the total voltage amplitude and the adjustable phase angle between the harmonics, respectively, and $\omega_{\mathrm{rf}} = 2\pi f$ with f being the fundamental frequency. It has been shown in investigations of low-pressure argon discharges that the resulting dc self-bias voltage is an almost linear function of the phase angle for $0^\circ \leqslant \theta \leqslant 90^\circ$ [26, 27] and is associated with a control of the mean sheath voltages. This, in turn, allows one to control the ion energies at both the powered and the grounded surfaces in geometrically symmetric or asymmetric discharges, while the ion flux remains approximately constant [26–32]. Here, only the special case of equal voltage amplitudes (see equation (1)) is considered.

This study focuses on the control of the IDFs at the electrodes of capacitively coupled high-pressure hydrogen discharges. With a small admixture of SiH_4, these discharges are typically used for silicon thin film deposition purposes [6, 8–12, 14]. In the following chapter, the setup of experiment and simulation as well as the modeling approach are introduced. Then, the dependence of the IDF on the gas pressure and the applied voltage amplitude is investigated in the third section, which is concluded by a discussion of the effectiveness of the Electrical Asymmetry Effect (EAE) under these conditions. Finally, a summary of the findings is given.

2. Description of experiment, simulation, and model

2.1. Experimental setup and diagnostics

The experimental setup has been described in detail previously [33]. In brief, the rectangular powered showerhead electrode with an edge length of 40 cm is separated from the grounded counterelectrode by a gap of 1.4 cm. Thus, the discharge configuration is geometrically symmetric and the dc self-bias vanishes under single frequency operation. The applied voltage is either a pure 13.56 MHz sine wave or a superposition of 13.56 MHz and 27.12 MHz according to the EAE and equation (1), respectively. The applied voltage is measured by a high-voltage probe, which is connected to the back side of the powered electrode.

The ion flux-energy distribution function is measured by a Balzer Plasma Process Monitor (PPM422) [34], which is implemented into the center of the grounded electrode. In principal, the measurement unit of the device consists of a set of ion optics, a cylindrical mirror analyzer of the ion energy and a quadrupole mass filter. Due to the high pressure in the discharge chamber, two pump stages are used. The base pressure in the measurement unit of the device was about 10^{-3} Pa. The first orifice (between the plasma and the intermediate pressure region) has a diameter of 100 μm and is grounded to prevent disturbances of the plasma. The second orifice (500 μm diameter) is located 15 mm behind the first orifice and is biased negatively to accelerate the ion beam into the focusing ion optics. Due to the highly collisional movement in the sheath, the IDF can be expected to have a rather broad angular distribution [35–37], which is not entirely captured by the acceptance angle of the device. By applying a high potential of -300 V to the second orifice, collisions of the ions with the background gas become improbable and the acceptance angle becomes wider. The measured species is H_3^+. Under all conditions investigated here the contribution of any other species to the total ion flux is negligible [38]. The PPM 422 is sensitive to the ion kinetic energy, ε_z, according to the velocity component perpendicular to the electrode surface (z-component) only. The settings of the energy filter are calibrated according to a procedure described in the literature [26, 34]. However, there is no calibration procedure for the shape of the IDF at elevated pressures and, hence, even after optimization of all settings the measurement uncertainty in the shape cannot be eliminated.

2.2. Hybrid Plasma Equipment Model simulation

The experimentally obtained shape of the IDF is benchmarked by the outcome of simulations using the Hybrid Plasma Equipment Model (HPEM) [39–41] by Mark Kushner's group. This two-dimensional simulation tool consists of several modules which address different physical phenomena. Reference [39] gives a good overview of the modules and related equations, so here, we will only present the used modules. We make use of the electron energy transport module (EETM) to obtain the electron energy distribution functions and electron-impact source functions. Within the fluid kinetics-Poisson module (FKPM), the electric field is determined and the electron fluxes are calculated using a drift–diffusion approximation. This is justified by the high collision frequency of about $5 \times 10^9\ \mathrm{s}^{-1}$ at 200 Pa compared with the driving frequency. In order to compute the transport and the distribution functions of H_3^+, the plasma chemistry Monte Carlo module (PCMCM) and the cross sections given by Phelps [43] have been utilized. Here, elastic collisions and collisionally induced dissociation are taken into account. The transport of the H^+ and H_2^+ ions is deduced from the momentum balance equation, and their temperatures are obtained via the energy balance equation. This means a simplification and, accordingly, a reduction in computational effort. The density of H^+ and H_2^+ is much smaller compared with the H_3^+ density [38, 56], so that the results are basically unaffected. The temperature of neutrals is kept constant at 300 K. For their transport, a diffusion approximation was used, resulting in an effectively constant gas background of the feed gas H_2. Since we do not expect electromagnetic effects at these frequencies [62], the electric potential and fields are obtained by solving Poisson's equation. In the EETM, we opted for the electron Monte Carlo simulation which is described in [42].

There are some differences between the experimental setup and the simulation. First of all, the fundamental frequency is not 13.56 MHz, but 10 MHz to simplify the time

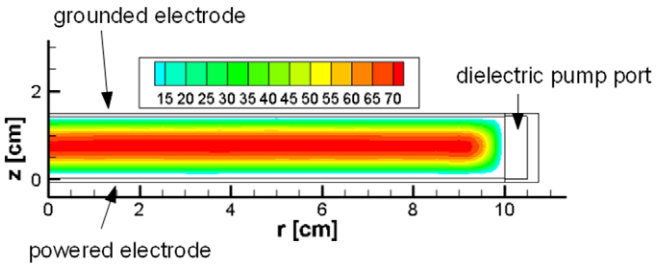

Figure 1. Sketch of the simulated discharge configuration. The powered electrode has a length of 20 cm and is separated from the grounded electrode by 1.4 cm. In the discharge volume the potential distribution is visualized. The color scale gives absolute values in volts for a pure hydrogen discharge operated at 200 Pa and an applied voltage of 200 V at 10 MHz.

scale. Secondly, the mesh differs from the actual reactor geometry. We kept the electrode distance of 1.4 cm and the rectangular shape of the electrodes. The electrode length is halved to 20 cm to save computational time. Furthermore, there is a dielectric pump port at the side wall (see figure 1). This improves the geometrical symmetry of the discharge and prevents artificially high electric fields at metal to metal corners or metal to dielectric planar boundaries.

2.3. Analytical model

In the following, a simple model approach for the IDF at the electrodes of a single frequency CCRF discharge is developed. In the energy interval $1\,\mathrm{eV} \leqslant \varepsilon_z \leqslant 30\,\mathrm{eV}$, the collision frequency of the H_3^+ ions with the H_2 background gas can be approximated to be independent of the incident ion energy. This is motivated by the fact that the cross section of elastic collisions is almost inversely proportional to the ion velocity in the respective interval [44], so that the product of cross section and velocity remains approximately constant. Then, the probability for an ion starting at $z = z_c$ to reach the electrode at $z = 0$ without undergoing a collision is $P(z) \propto \exp(-\nu\tau_z(z_c))$. Here, ν is the collision frequency and $\tau_z(z_c)$ is the time interval between the last collision and the arrival at the electrode. In practical terms, we set

$$\nu \approx p[\mathrm{Pa}]/(1.5 \times 10^{-6}\,\mathrm{s}) \tag{2}$$

with p the neutral gas pressure in Pa. Within the ion energy range discussed here, the distance an ion moves between subsequent collisions is small compared with the sheath width. In other words, the ion transit time [3–5] is much larger than τ_z. Thus, the major part of the ion momentum gained in the field is lost in collisions. This is strictly valid for ions and neutrals of equal mass and can be expected to hold for H_3^+ ions colliding with H_2 neutrals, as the mass ratio of 1.5 still allows for an efficient momentum transfer. Accordingly, in our model the ions start at the position of the last collision z_c close to the electrode with a negligible energy. Then, they become accelerated over the distance z_c, over which the electric field changes only weakly. This allows us to approximate the electric field close to the electrode by its value at $z = 0$, i.e. any spatial dependence within the last mean free path is neglected. In a symmetric discharge driven by a single frequency, f, the temporal evolution of the sheath electric field and voltage drop can be approximated to vary as $\cos^2(\varphi/2)$, where $\varphi = \omega_{\mathrm{rf}} t = 2\pi f t$ is the rf phase.

The acceleration of an ion starting at rest at phase φ_0, at the position z_c of the last collision in the sheath by the electric field $E \approx E_0 \cos^2(\varphi/2)$ leads to an ion velocity directed toward the electrode surface of

$$v_z(\varphi) = \frac{eE_0}{m_i\omega_{\mathrm{rf}}} \int_{\varphi_0}^{\varphi_0+\omega_{\mathrm{rf}}\tau_z} \cos^2\left(\frac{\varphi}{2}\right) \mathrm{d}\varphi. \tag{3}$$

Again, we make use of the frequency scaling, i.e. the change in the electric field during the time of free ion flight, τ_z, is neglected, as the collision frequency is about one order of magnitude larger than the applied radio frequency under the relatively high-pressure conditions considered in this work. Thus, the velocity is

$$v_z(\varphi_0) \approx \frac{eE_0}{m_i\omega_{\mathrm{rf}}} \cos^2\left(\frac{\varphi_0}{2}\right) \omega_{\mathrm{rf}}\tau_z. \tag{4}$$

Rearranging equation (4) and introducing the kinetic ion energy according to the velocity component perpendicular to the electrode surface, $\varepsilon_z = m_i v_z^2/2$, yields

$$\tau_z(\varepsilon_z, \varphi_0) \approx \frac{\sqrt{2\varepsilon_z m_i}}{eE_0 \cos^2(\varphi_0/2)}. \tag{5}$$

Finally, the shape of the time averaged distribution function, $\langle P(\varepsilon_z)\rangle$, is found by integrating the probability $P(\varepsilon_z, \varphi) \propto \exp(-\nu\tau_z(\varepsilon_z, \varphi_0))$ over the rf period. It is assumed that the incoming ions are equally distributed over all starting phases before the last collision, φ_0. The integration can be performed analytically by substituting $\cos^{-2}(\varphi_0/2) = 1 + \tan^2(\varphi/2) = 1 + u^2$. The result is

$$\langle P(\varepsilon_z)\rangle \propto \frac{1}{2\pi} \int_0^{2\pi} \exp\left\{-\frac{\nu\sqrt{2\varepsilon_z m_i}}{eE_0 \cos^2(\varphi_0/2)}\right\} \mathrm{d}\varphi_0 \tag{6}$$

$$\propto \frac{4}{3\varepsilon_c} \mathrm{erfc}\left(\sqrt{\frac{\nu}{eE_0}\sqrt{2m_i\varepsilon_z}}\right) \tag{7}$$

$$= \frac{4}{3\varepsilon_c} \mathrm{erfc}\left[\left(\frac{\varepsilon_z}{\varepsilon_c}\right)^{1/4}\right], \tag{8}$$

the complementary error function with an argument scaling with $\varepsilon_z^{1/4}$. The factor $4/(3\varepsilon_c)$ is required for normalization by the total flux, i.e. to achieve $\int_0^\infty \langle P(\varepsilon_z)\rangle\,\mathrm{d}\varepsilon_z = 1$. It should be noted that basically the same expression can be deduced from the energy gain in the potential instead of the momentum gain due to the acceleration in the sheath electric field [63]. This formula (equation (8)) allows for an understanding of the dependence of the IDF on a global parameter

$$\varepsilon_c = \frac{1}{2} m_i \left(\frac{eE_0}{\nu m_i}\right)^2. \tag{9}$$

To give a dependence on practical units the electric field strength at the electrode is $E_0 \approx 2\phi_0/s_{\max}$ in the approximation of the matrix sheath model, which assumes a constant and homogeneous ion density in the sheath. Here, ϕ_0 is the

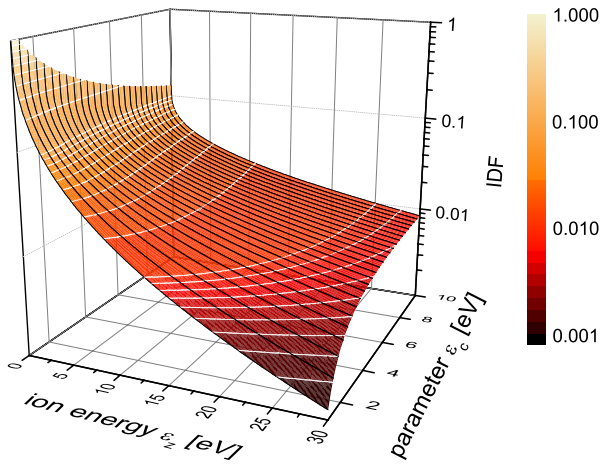

Figure 2. IDF resulting from the model as a function of the energy ε_z and parameter ε_c.

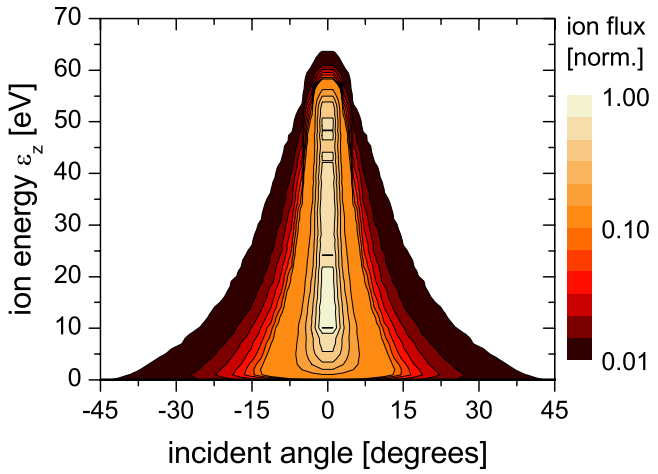

Figure 3. Normalized ion flux-energy angular distribution function resulting from the simulation at 200 Pa and a voltage amplitude of 200 V. The flux of ions at angles larger than $|\theta_i| = 45°$ is negligible.

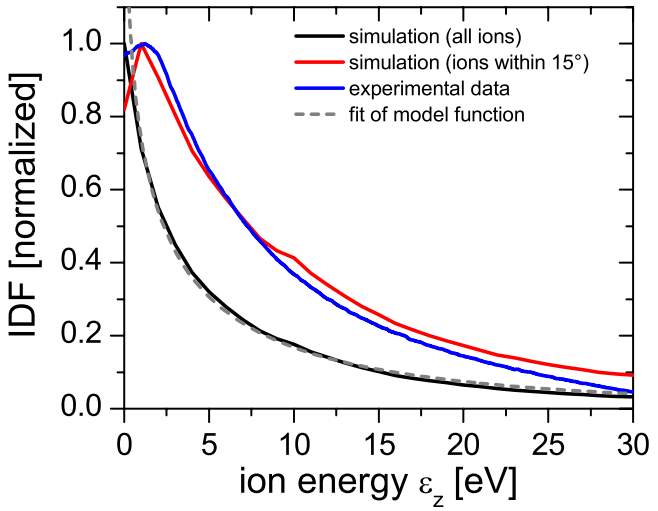

Figure 4. Normalized ion flux-energy distribution function obtained experimentally, by the HPEM simulation, and in the analytical model. In the simulation, the entire angular distribution function (black curve) or all ions with an incident angle of 15° or less (red curve) are evaluated. The pressure is 200 Pa and the applied voltage is 200 V.

amplitude of the applied rf voltage and s_{max} is the maximum sheath extension. In other words, the simple matrix model (see, e.g., p 65 in [2] or p 175 in [1]) neglects the acceleration of ions, which is motivated by the high collision frequency, and ionization within the sheath. Then, the global parameter becomes

$$\varepsilon_c = \frac{1}{2m_i}\left(\frac{e\phi_0}{\nu s_{max}}\right)^2, \qquad (10)$$

which resembles the fundamental parameter in drift studies, e.g. in theories on the IDF in homogeneous electric fields [45–48]. In fact, it differs from the mean drift energy [45–47] only by a numerical factor, taking the difference between the maximum and mean field strength into account. In our case, typical values for ε_c are in the range 2–5 eV. Figure 2 shows the IDF resulting from the model (equation (8)) in the energy range $0\,\text{eV} \leqslant \varepsilon_z \leqslant 30\,\text{eV}$ for values of ε_c in the range between 1 eV and 10 eV. As one might expect, the parameter ε_c determines the steepness of the distribution function, i.e. the IDF will become broader and will show an enhanced tail, if the gain in ε_z becomes larger due to a stronger electric field and the loss in ε_z becomes smaller, i.e. τ_z becomes larger, due to a lower collision frequency. In the next section, equation (8) will be compared with simulation data.

3. Results

At first, the normalized ion flux-energy angular distribution function resulting from the simulation is shown in figure 3. Here, the total ion flux Γ_i is analyzed with respect to the energy ε_z and the solid angle, i.e. the distribution function is computed as $\sqrt{\varepsilon_z}\mathrm{d}^2\Gamma_i/(\sin\theta_i \mathrm{d}\theta_i \mathrm{d}\varepsilon_z)$ with θ_i being the azimuth angle. Ions arriving with small energies ε_z are likely to have undergone collisions directly before reaching the electrode, in which the incident energy gained in the sheath electric field has been redistributed. In contrast, ions impinging on the electrode with relatively high energies ε_z had a relatively long time of free flight compared with the statistical average. Thus, the direction of motion of these ions is dominated by the direction of the electric field, so that large angles are physically not possible. Therefore, the angular distribution function shows the typical shape of a broad distribution at small energy, that becomes narrower with increasing ε_z [35]. The ion energy, according to the velocity component lateral to the electrode surface, gives a considerable contribution to the total energy impact at the surface and might be important for applications, depending on thresholds of surface processes, for instance [35–37, 55].

The comparison of the simulation results with a fit of the model function (equation (8)) to the simulation data in the range $1\,\text{eV} \leqslant \varepsilon_z \leqslant 30\,\text{eV}$ and the measured distribution function at 200 Pa is depicted in figure 4. Excellent agreement regarding the shape of the IDF resulting from simulation and model is found. The obtained fit parameter is $\varepsilon_c \approx 3.69$. Setting the collision frequency to $1.33 \times 10^8\,\text{s}^{-1}$ according to equation (2) and taking the applied voltage amplitude of 200 V, this value corresponds to a maximum sheath width of about

6.3 mm, which agrees very well with the value determined in the self-consistent simulation ($s_{max} = 6.2$ mm). Only at very small energies, i.e. below 1 eV where the model is not expected to be valid, the flux is overestimated. The distribution function has a maximum of about 2.4 at $\varepsilon_z = 0$; as all IDFs are normalized by their maximum in figure 4, the distribution function obtained by the fit of the model function is not normalized by the total flux.

Therefore, the model allows for an analytical treatment of the distribution function and might even be used in a predictive way, despite the drastic simplification made in its derivation. In fact, the shape of the IDF is similar to the distributions obtained in simulations of dc discharges in hydrogen [49], justifying the model approach chosen here. The measured IDF shows a deviation from the angle integrated simulation and model data, respectively. This is caused by the finite acceptance angle of the measurement device, which inhibits a direct comparison [32, 50, 51]. As shown in the figure, a distribution function resulting from those ions, which arrive under an angle of 15° or less with respect to the electrode surface normal in the simulation, reasonably follows the measured trend. This acceptance angle roughly matches an estimation based on geometrical considerations of the distance and diameter of the entrance orifices. It should be noted that the acceptance angle itself may generally depend on the ion energy according to the velocity component perpendicular to the electrode surface, ε_z [50]. On the one hand, the reliability of the experimental data is limited by the measurement approach. On the other hand, the validity of numerical codes can only be proven by direct comparisons of simulation data to experimental results [50, 64]. Further studies on energy-resolved mass spectrometry are required to provide a concluding discussion. Nevertheless, the comparison shown in figure 4 confirms that the measurements give an important experimental insight into the ion distribution functions in capacitive hydrogen discharges under these conditions, i.e. at relatively high pressures.

In the following we investigate the dependence of the measured IDF on global discharge parameters, such as pressure as well as amplitude and shape of the applied voltage waveform, respectively. By comparing this fraction of the distribution function with the fully angle-integrated IDF resulting from the simulation (see figure 4), it can be concluded that most of the ions arriving under large angles have a small energy ε_z. Moreover, a small structure at about 10 eV is observed, which is due to the ion motion in a periodically oscillating sheath, similar to specific features of ion distribution functions under low-pressure conditions (see, e.g. [3, 4, 51–54] and references therein).

Figure 5 shows the normalized IDF obtained experimentally for various gas pressures. All functions are normalized by their respective maximum. The applied voltage is 200 V at 13.56 MHz. As discussed above, the IDF exhibits a maximum at very low energies and not at $\varepsilon_z = 0$ because of the finite acceptance angle. Then, it declines monotonically as a function of ε_z within this high pressure range [54]. These results are in contrast to the experimental results presented for similar pressures and higher applied frequencies in the literature [38, 56]. The discrepancy might be due to the fact

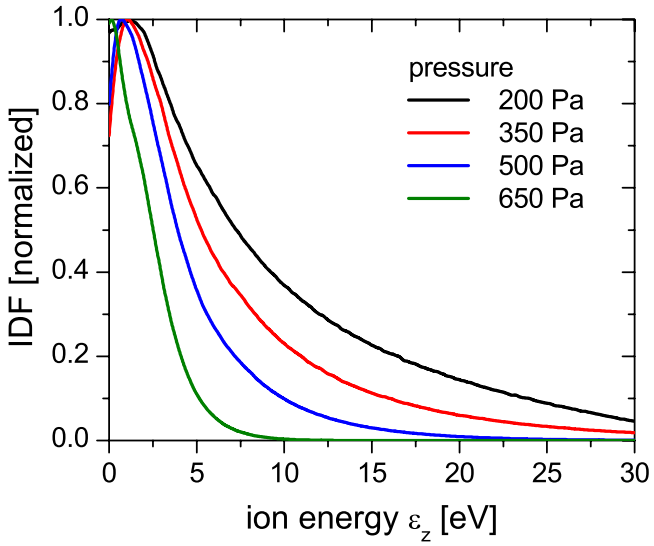

Figure 5. Normalized ion flux-energy distribution function obtained experimentally for various gas pressures. The applied voltage is 200 V at 13.56 MHz.

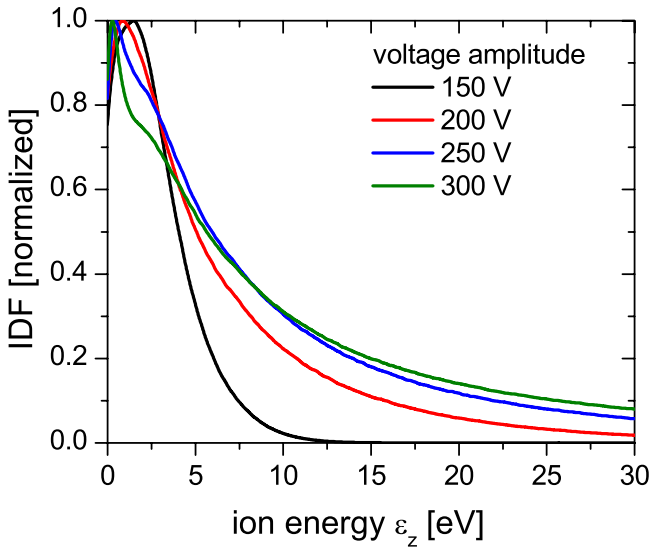

Figure 6. Normalized ion flux-energy distribution function obtained experimentally for various voltage amplitudes at 13.56 MHz. The gas pressure is 350 Pa.

that the measurement device is implemented into the grounded surface in our case, whereas it is not directly connected to ground in the other studies. Ions with relatively high energies (e.g. about 30 eV) give a significant contribution only at pressures below 200 Pa. With increasing pressure, the ion mean free path decreases more strongly than the sheath extension [57]. Therefore, the ion motion in the sheath becomes more collisional and the width of the maximum in the measured distribution is reduced [54]. From these results, we can conclude that the width of the IDF scales inversely proportional with pressure.

Figure 6 shows the normalized IDF obtained experimentally for various voltage amplitudes at a constant gas pressure of 350 Pa. The high-energy tail of the peak is enhanced with increasing voltage. This is due to the fact that

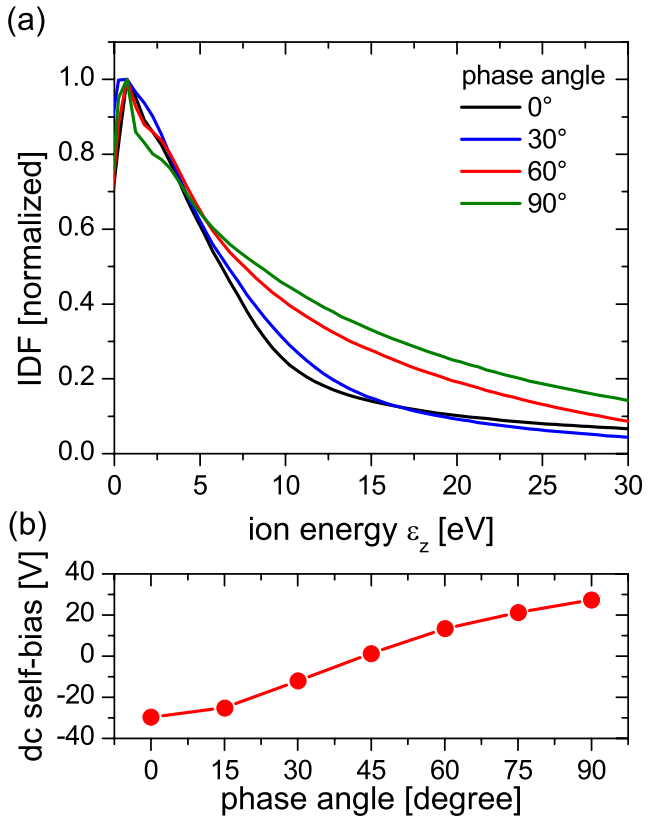

Figure 7. (*a*) Normalized ion flux-energy distribution function and (*b*) dc self-bias measured for different phase angles at 350 Pa and $\phi_0 = 200$ V.

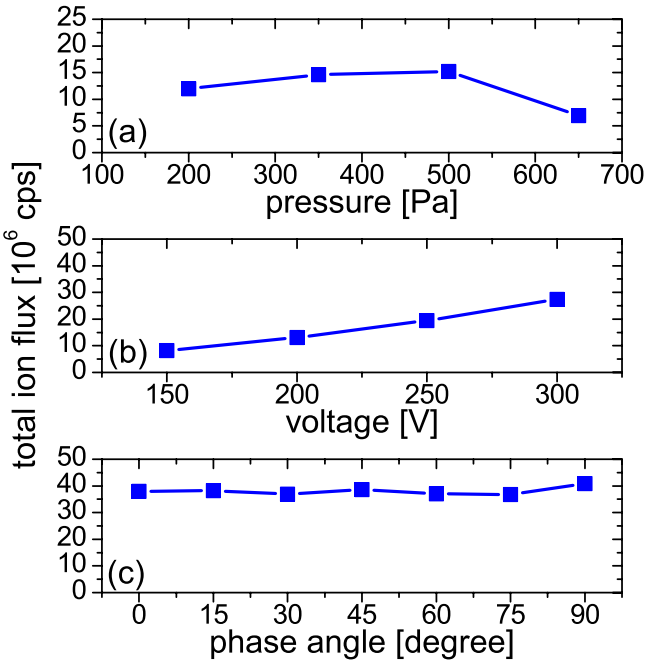

Figure 8. Measured total ion flux for various pressures and voltages in a single frequency discharge as well as for different phase angles in an electrically asymmetric dual frequency discharge. The conditions in (*a*), (*b*) and (*c*) are the same as in figures 5, 6 and 7, respectively.

the sheath electric field ($E_0 \approx 2\phi_0/s_{max}$ in the approximation of the matrix sheath model) becomes higher as ϕ_0 is increased and the increase in the sheath width is only moderate due to the increase in the plasma density [54, 57]. Similarly, this would correspond to an increase in ε_c in the model (see equation (8) and figure 2). The fraction of the IDF having a relatively high energy increases strongly from $\phi_0 = 150$ V to $\phi_0 = 200$ V and shows only a minor increase from $\phi_0 = 250$ V to $\phi_0 = 300$ V. In addition to changes in the sheath width, the fraction of ions produced by highly energetic electrons in the sheath, which are heated by a local field reversal in the sheath region at the time of sheath collapse [58–61], might probably depend on the voltage amplitude. Therefore, the sheath electric field depends on ϕ_0 in a nonlinear way and the complete sheath structure is affected by the applied voltage amplitude. Such effects are not captured by the model.

Using the EAE, the IDF can be manipulated at constant pressure and voltage amplitude by adjusting the phase angle θ [26, 31]. Figure 7(*a*) presents the normalized ion flux-energy distribution function measured for different phase angles at 350 Pa and $\phi_0 = 200$ V. Both the width and the shape of the distribution function change, because the temporal dependence of the sheath electric field changes [27], i.e. it is relatively high for a small (large) fraction of the rf period at the grounded side for $\theta = 0^\circ$ ($\theta = 90^\circ$). The behavior of the ions in such fields consisting of many Fourier components is a current topic in both analytical and numerical sheath theory [5, 18]. In general, the right shoulder of the peak is higher than the one in a 13.56 MHz discharge under otherwise identical conditions, because the combination of this frequency with higher harmonics produces a higher plasma density [30] and, therefore, reduces the collisionality due to the diminished sheath width [28]. In agreement with the maximum positive dc self-bias at $\theta = 90^\circ$ (see figure 7(*b*)), the mean sheath voltage and ion energy are highest in this case at the grounded electrode [26–29, 31, 33].

According to the results presented in figures 5, 6, and 7 the shape of the IDF changes with global control parameters such as pressure, voltage or electrical symmetry. As shown in figure 8, the total ion flux weakly depends on the gas pressure and strongly increases as a function of the applied voltage amplitude [54].

The pressure dependence shows a maximum [38], which might be attributed to changes in the total absorbed power as well as to the various collision processes of highly energetic electrons: if the pressure is increased, the collision frequency will be further enlarged so that the energy gain of electrons, e.g. via the interaction with the sheath electric field, between collisions becomes smaller and fewer electrons reach an energy according to the ionization threshold. This would lead to a decreasing trend of the ion flux as a function of pressure. However, the dependences of the plasma density profile and power absorption on pressure at constant applied voltage amplitude preclude a definite explanation. If the applied voltage amplitude is increased, the power deposited into the discharge volume will increase. Therefore, the electron heating becomes stronger leading to an increased plasma density. These reasonings might explain why the plasma density and, as a consequence thereof, the ion flux

depend on pressure and voltage, respectively. However, the ion flux might be expected to remain approximately constant, if the phase angle is used as the control parameter for the IDF, due to the almost constant electron power absorption for all θ [27, 29]. The independent control of ion energy and ion flux via the EAE has been proven for the case of low-pressure electropositive discharges [29]. However, the total ion flux can be expected to have a phase angle dependence, if the electron heating dynamics change. This could be the fact under certain conditions, which lead to a mode transition from the α-mode (sheath expansion heating) to the γ-mode (ionization by secondary electrons) [23]. In addition, the ion flux will depend on the phase angle if the electron heating by field reversals [58–61] close to the electrode, i.e. deep inside the sheath region, becomes the dominant source of ionizing electrons and, therefore, leads to a violation of ion flux conservation within the sheath. Therefore, the dependence of the ion flux on global control parameters is complex and a detailed study as well as a validation of the constancy of the ion flux found here is planned in future simulations. Based on the measurement results presented above, the properties of the ions at the surface can be controlled independently under the conditions of high pressure and relatively low voltage amplitudes considered in this work using the EAE.

4. Conclusions

The flux-energy distribution functions of the ions flowing onto the electrodes in high-pressure CCRF discharges operated in hydrogen are measured under single and dual frequency discharge operation. The measurements are performed for the first time under high-pressure conditions in a 13.56 MHz as well as in an electrically asymmetric discharge. We find that the shape of the IDF exhibits an almost exponentially decaying behavior due to the high collision probability of the H_3^+ ions during their acceleration by the sheath electric field. A simple analytical model reasonably reproduces the IDF obtained by a HPEM simulation. In single frequency discharges, the results of both experiment and model show that the width of the distribution function increases with voltage and decreases with pressure. Using the electrical asymmetry effect (EAE) in dual frequency discharges, the shape and the width of the IDF depend on the phase angle between the applied harmonics. In contrast to the variation of gas pressure or applied voltage amplitude, the EAE is observed to control the IDF without changing the total ion flux. This separate control is of fundamental interest for both research, e.g. examining the role of the shape of the IDF on surface processes under otherwise identical conditions, and applications such as the large area deposition of thin films [6–9, 10, 14].

Acknowledgments

Funding by the German Federal Ministry for the Environment, Nature conservation, and Nuclear Safety (0325210B) and the Ruhr-University Research Department Plasma is gratefully acknowledged.

References

[1] Lieberman M A and Lichtenberg A J 2005 *Principles of Plasma Discharges and Materials Processing* 2nd edn (Hoboken, NJ: Wiley)
[2] Chabert P and Braithwaite N 2011 *Physics of Radio-Frequency Plasmas* (New York: Cambridge University Press)
[3] Kawamura E, Vahedi V, Lieberman M A and Birdsall C K 1999 *Plasma Sources Sci. Technol.* **8** R45
[4] Xiang N and Waelbroeck F L 2005 *Phys. Plasmas* **12** 033505
[5] Donkó Z and Petrović Z Lj 2007 *J. Phys.: Conf. Ser.* **86** 012011
[6] Roschek T, Repmann T, Müller J, Rech B and Wagner H 2002 *J. Vac. Sci. Technol.* A **20** 492
[7] Martinu L, Klemberg-Sapieha J E, Küttel O M, Raveh A and Wertheimer M R 1994 *J. Vac. Sci. Technol.* A **12** 1360
[8] Kalache B, Kosarev A I, Vanderhaghen R and Roca i Cabarrocas P 2003 *J. Appl. Phys.* **93** 1262
[9] Nozawa R, Takeda H, Ito M, Hori M and Goto T 1997 *J. Appl. Phys.* **81** 8035
[10] Katsia E, Amanatides E, Mataras D, Soto A and Voyiatzis G A 2005 *Sol. Energy Mater. Sol. Cells* **87** 157
[11] Johnson E V, Verbeke T, Vanel J-C and Booth J-P 2010 *J. Phys. D: Appl. Phys.* **43** 412001
[12] Johnson E V, Pouliquen S, Delattre P A and Booth J-P 2012 *J. Non-Cryst. Solids* **358** 1974
[13] Amanatides E, Katsia E, Mataras D, Soto A and Voyiatzis G A 2006 *Thin Solid Films* **511** 603
[14] Hrunski D *et al* 2013 *Vacuum* **87** 114
[15] Wang S-B and Wendt A E 2000 *J. Appl. Phys.* **88** 643
[16] Diomede P, Economou D J and Donelly V M 2011 *J. Appl. Phys.* **109** 083302
[17] Boyle P C, Ellingboe A R and Turner M M 2004 *J. Phys. D: Appl. Phys.* **37** 697
[18] Wu A C F, Lieberman M A and Verboncoeur J P 2007 *J. Appl. Phys.* **101** 056105
[19] Gans T, Schulze J, O'Connell D, Czarnetzki U, Faulkner R, Ellingboe A R and Turner M M 2006 *Appl. Phys. Lett.* **89** 261502
[20] Turner M M and Chabert P 2006 *Phys. Rev. Lett.* **96** 261502
[21] Schulze J, Gans T, O'Connell D, Czarnetzki U, Ellingboe A R and Turner M M 2007 *J. Phys. D: Appl. Phys.* **40** 7008
[22] Donkó Z, Schulze J, Hartmann P, Korolov I, Czarnetzki U and Schüngel E 2010 *Appl. Phys. Lett.* **97** 081501
[23] Schulze J, Donk´o Z, Schuengel E and Czarnetzki U 2011 *Plasma Sourc. Sci. Technol.* **20** 045007
[24] Booth J P, Curley G, Marić D and Chabert P 2010 *Plasma Sources Sci. Technol.* **19** 015005
[25] Heil B G, Czarnetzki U, Brinkmann R P and Mussenbrock T 2008 *J. Phys. D: Appl. Phys* **41** 165202
[26] Schulze J, Schüngel E and Czarnetzki U 2009 *J. Phys. D: Appl. Phys* **42** 092005
[27] Czarnetzki U, Schulze J, Schüngel E and Donkó Z 2011 *Plasma Sources Sci. Technol.* **20** 024010
[28] Schulze J, Schüngel E, Donkó Z and Czarnetzki U 2011 *Plasma Sources Sci. Technol.* **20** 015017
[29] Schüngel E, Schulze J, Donkó Z and Czarnetzki U 2011 *Phys. Plasmas* **18** 013503
[30] Lafleur T, Delattre P A, Johnson E V and Booth J-P 2012 *Appl. Phys. Lett.* **101** 124104
[31] Schüngel E, Eremin D, Schulze J, Mussenbrock T and Czarnetzki U 2012 *J. Appl. Phys.* **112** 053302
[32] Delattre P-A, Lafleur T, Johnson E and Booth J-P 2013 *J. Phys. D: Appl. Phys.* **46** 235201
[33] Schüngel E, Mohr S, Iwashita S, Schulze J and Czarnetzki U 2013 *J. Phys. D: Appl. Phys.* **46** 175205
[34] Balzers Instruments 1998 Operation manual of Plasma Process Monitor DG 803813 BE (9808) www.bi.balzers.com/library/gasana

[35] Kushner M J 1985 *J. Appl. Phys.* **58** 4024
[36] Liu J, Huppert G L and Sawin H H 1990 *J. Appl. Phys.* **68** 3916
[37] Myers F R, Ramaswami M, Cale T S 1994 *J. Electrochem. Soc.* **141** 1313
[38] Nunomura S and Kondo M 2007 *J. Appl. Phys.* **102** 093306
[39] Kushner M J 2009 *J. Phys. D: Appl. Phys.* **42** 194013
[40] Wang M and Kushner M J 2011 *J. Vac. Sci. Technol.* A **29** 051306
[41] Shoev J and Kushner M J 2011 *J. Vac. Sci. Technol.* A **29** 051305
[42] Ventzek P L G, Hoekstra R J and Kushner M J 1993 *J. Vac. Sci. Technol.* A **B12** 461
[43] Phelps A V http://jilawww.colorado.edu/ avp/collision data/ unpublished
[44] Phelps A V 1990 *J. Phys. Chem. Ref. Data* **19** 653
[45] Whealton J H and Woo S-B 1971 *Phys. Rev.* A **6** 2319
[46] Lampe M, Röcker T B, Joyce G, Zhdanov S K, Ivlev A V and Morfill G E 2012 *Phys. Plasmas* **19** 113703
[47] Kuhn S 1980 *Phys. Rev.* A **22** 2460
[48] Wannier G H 1941 *Phys. Rev.* **83** 281
[49] Bretagne J, Gousset G, and Simko T 1994 *J. Phys. D: Appl. Phys.* **27** 1866
[50] O'Connell D, Zorat R, Ellingboe A R and Turner M M 2007 *Phys. Plasmas* **14** 103510
[51] Diomede P, Longo S, Economou D J and Capitelli M 2012 *J. Phys. D: Appl. Phys.* **45** 175204
[52] Wild C and Koidl P 1991 *J. Appl. Phys.* **69** 2909
[53] Israel D, Riemann K-U and Tsendin L 2006 *J. Appl. Phys.* **99** 093303
[54] Donkó Z, Schulze J, Czarnetzki U, Derzsi A, Hartmann P, Korolov I and Schüngel E 2012 *Plasma Phys. Control. Fusion* **54** 124003
[55] Woodworth J R, Riley M E, Miller P A, Nichols C A and Hamilton T W 1997 *J. Vac. Sci. Technol.* A **15** 3015
[56] Muta H, Kishida S, Tanaka M, Yamauchi Y, Baba T, Takeuchi Y, Takatsuka H and Kawai Y 2009 *Plasma Process. Polym.* **6** S792
[57] Mutsukura N, Kobayashi K and Machi Y 1990 *J. Appl. Phys.* **68** 2657
[58] Schulze J, Schüngel E, Donkó Z, Luggenhölscher D and Czarnetzki U 2010 *J. Phys. D: Appl. Phys.* **43** 124016
[59] Mahony C M O, Wazzan R A and Graham W G 1997 *Appl. Phys. Lett.* **71** 608
[60] Schulze J, Donkó Z, Heil B G, Luggenhölscher D, Mussenbrock T, Brinkmann R P and Czarnetzki U 2008 *J. Phys. D: Appl. Phys.* **41** 105214
[61] Czarnetzki U, Luggenhölscher D and Döbele H F 1999 *Plasma Sources Sci. Technol.* **8** 230
[62] Perret A, Chabert P, Booth J-P, Jolly J, Guillon J and Auvray Ph 2003 *Appl. Phys. Lett.* **83** 243
[63] Schüngel E 2013 *PhD Thesis* Ruhr-University Bochum
[64] Zhang Y, Kushner M J, Moore N, Pribyl P and Gekelman W 2013 *J. Vac. Sci. Technol.* A **31** 061311